Rheol Acta (2008) 47:49–62
DOI 10.1007/s00397-007-0207-6

ORIGINAL CONTRIBUTION

Numerical simulation of the extrusion of strongly compressible Newtonian liquids

Eleni Taliadorou · Georgios C. Georgiou · Evan Mitsoulis

Received: 21 January 2007 / Accepted: 28 April 2007 / Published online: 4 June 2007
© Springer-Verlag 2007

Abstract The axisymmetric and plane extrusion flows of a liquid foam are simulated assuming that the foam is a homogeneous compressible Newtonian fluid that slips along the walls. Compressibility effects are investigated using both a linear and an exponential equation of state. The numerical results confirm previous reports that the swelling of the extrudate decreases initially as the compressibility of the fluid is increased and then increases considerably. The latter increase is sharper in the case of the exponential equation of state. In the case of non-zero inertia, high compressibility was found to lead to a contraction of the extrudate after the initial expansion, similar to that observed experimentally with liquid foams and to decaying oscillations of the extrudate surface. The time-dependent calculations show that the oscillatory steady-state solutions are stable. These steady-state oscillatory solutions are not affected by the length of the extrudate region nor by the boundary condition along the wall.

Keywords Newtonian flow · Extrudate swell flow · Compressibility · Slip · Liquid foams

E. Taliadorou · G. C. Georgiou (✉)
Department of Mathematics and Statistics, University of Cyprus, P.O. Box 20537, 1678 Nicosia, Cyprus
e-mail: georgios@ucy.ac.cy

E. Mitsoulis
School of Mining Engineering and Metallurgy, National Technical University of Athens, Heroon Polytechneiou 9, 15780 Zografou, Athens, Greece

Introduction

Foams are structured dispersions of gas bubbles in a small volume fraction of a liquid with the liquid as the continuous phase and the gas as the dispersed one. Foamed products are useful in many different industrial applications. In the plastics industry, polyethylene, polystyrene, and polypropylene foams are produced for thermal insulation, packaging applications, protecting and sporting equipment, and aircraft or automotive parts with high strength to weight ratio (Park et al. 1998; Naguib et al. 2004). Foamed polymer solutions are used widely in the petroleum industry as drilling fluids and in the hydraulic fracturing of hydrocarbon wells (Gardiner et al. 1999). Metal foams also find applications in the automotive industry (Belkessam and Fritsching 2003). Aqueous polymer solutions foamed with nitrogen and/or carbon dioxide are used in fire-fighting technology for polar solvent and oil fires (Gardiner er al. 1999; Höhler and Cohen-Addad 2005). Other applications can be found in the food and biopolymer industry, with products ranging from starch-based foams Willett and Shogren (2002), cereal foods (Moraru and Kokini 2003; Wang et al. 2005),and aerated chocolates (Gardiner et al. 1999) to cosmetics and medical drugs (Höhler and Cohen-Addad 2005).

In foam extrusion, a chemical foaming agent is mixed with the polymer to be extruded. The heat generated to melt the polymer decomposes the chemical foaming agent producing gas, which is dispersed in the polymer melt. An alternative is to blow the polymer melt with an inert gas, such as carbon dioxide or nitrogen (Park et al. 1998; Xu et al. 2003; Naguib et al. 2004). Upon exiting the die, the gas expands considerably. Expansion of

extrudates is one of the most important phenomena of foam extrusion processing, resulting in products with a cellular foam structure (Wang et al. 2005; Naguib et al. 2004; Naguib et al. 2006). This is a complex phenomenon caused by different mechanisms, such as phase transitions, nucleation, and bubble growth and collapse (Moraru and Kokini 2003; Naguib et al. 2004; Naguib et al. 2006) in addition to extrudate swell. Important parameters that affect the final dimensions and quality of the extrudate are the die geometry, material properties, and processing environment (Wang et al. 2005).

In the polymer foam production industry, the expansion of the extrudate is usually described by the volume expansion ratio, which is also known as the overall expansion ratio or foaming ratio. This is the ratio of the extrudate solid density to the bulk density. In the food industry, the radial expansion ratio is used instead. This is the ratio of the cross-sectional area of the extrudate to that of the die (Sokhey et al. 1997; Xu and Hanna 2005). In other words, the radial expansion ratio is the square of the well-known extrudate swell ratio, which is defined as the ratio of the final extrudate diameter to that of the die. The axial expansion ratio calculated by dividing the volume expansion by the radial expansion ratio is also used (Sokhey et al. 1997). The expansion ratios and the density are important properties of extruded foams. High expansion ratios and low unit density are ideal for foams because of the reduced cost of the final product (Xu and Hanna 2005).

In general, polymer foams produced by conventional extrusion process exhibit high expansion ratios up to 100. Park et al. (1998) reported volume expansion ratios as high as 23 for microcellular high-impact polystyrene (HIPS) foams in the range of 1.5–20 for fine-cell high-density polyethylene (HDPE) foams (Behravesh et al. 1998) and up to 45 for biodegradable polyester foams (Park et al. 1999). For the extrusion of polypropylene foams blown with butane, Naguib et al. (2004); Naguib et al. (2006) reported that volume expansion ratios ranged from about 1 to 90, depending on the gas fraction, the temperature, and the talc content. Very recently, Lee et al. (2006) reported volume expansion ratios ranging from 2.3 to 8.5 in the case of open-cell low-density polyethylene/polystyrene (LDPE/PS) sheet foams produced with an annular die. Xu et al. (2005) reported volume expansion ratios up to 6 in direct extrusion foaming of a low-density polypropylene. Large expansion ratios are also observed in the case of extruded biodegradable starch and cereal foams. Radial expansion ratios up to 62.4 have been reported (Willett and Shogren 2002; Moraru and Kokini 2003; Xu and Hanna 2005).

Of particular interest to the present work is the phenomenon of the contraction of the extrudate after the initial expansion near the die exit, which is known to be detrimental to large expansion (Naguib et al. 2006). This contraction is attributed to the escape of gas through the exterior skin of the extruded foam (Behravesh et al. 1998; Park et al. 1998; Naguib et al. 2004). Therefore, to produce low-density foams, gas diffusion must be prevented. In extrusion experiments with microcellular HIPS foams blown with carbon dioxide, Park et al. (1998) observed that the diameter of the initially expanded foam at a relatively high temperature was about 2.2 times of the diameter of the finally contracted foam. By decreasing both the melt and nozzle temperatures, Park et al. (1998) were able to achieve full expansion, eliminating the contraction, which was attributed to the reduced gas diffusion through the frozen skin layer of the extrudate and the suppression of cell coalescence.

Naguib et al. (2004) and Naguib et al. (2006) studied the fundamental mechanisms governing the volume expansion behavior of extruded polypropylene foams blown with butane. Based on their experimental data, they reached the conclusion that either gas loss or polymer crystallization govern the final volume expansion ratio of the polypropylene foams and that the maximum expansion ratio was achieved when the governing mechanism changed from one to the other. They also noted that at higher temperatures, initial expansion is followed by an undesirable contraction and that as temperature is increased, initial expansion becomes larger but final expansion is reduced beyond an optimum temperature. The angle of initial expansion was found to increase with temperature, i.e., initial expansion becomes faster (Naguib et al. 2004).

Extrudate contraction after the initial expansion has also been observed with extruded starch-based foams (Fan et al. 1994; Willett and Shogren 2002; Wang et al. 2005; Xu and Hanna 2005) and cereal foods (Moraru and Kokini 2003), resulting in increased densities and reduced expansions. Willett and Shogren (2002) and Moraru and Kokini (2003) attribute this phenomenon to the cooling rate, which is not rapid enough to prevent bubble collapse.

The objective of the present work is to study numerically the expansion of extruded foams in the so-called extrudate swell flow and investigate whether the aforementioned phenomenon of extrudate contraction can be attributed to the compressibility of the foam. The latter is treated as a homogeneous fluid. In other words, the extrudate expansion of foamed liquids is studied at a macroscopic level. Bubble growth phenomena are taken into account implicitly by assuming that the foam

is highly compressible. For other analyses in which bubble growth is characterized at a microscopic level, the reader is referred to the paper by Wang et al. (2005) and the references therein.

The knowledge of the rheological behavior of foamed fluids is essential in engineering applications. As stated by Reinelt and Kraynik (2000), a complete theory of foam rheology does not exist, as foam behavior involves a broad range of physical mechanisms acting over multiple length and time scales. Additional information concerning these physical mechanisms can also be found in the recent review article of Höhler and Cohen-Addad (2005). Rheological studies have shown that foam viscosity depends on properties, such as the foam expansion ratio, defined as the ratio of the volume of the foam to the volume of the foam liquid at atmospheric conditions, the bubble size distribution, and other properties of individual phases, i.e., the surface tension (Enzendorfer et al. 1995; Gardiner et al. 1999). In general, a foam behaves like a non-Newtonian fluid exhibiting shear thinning, yield stress, and elastic behavior typical of emulsions (Kraynik 1988). The origin of the elastic behavior comes from the minimization of surface area due to the surface tension that exists in the thin liquid films. The yield stress arises due to the internal structure of foam, which consists of bubbles separated by a matrix of thin films (Kraynik 1988). Yield stress was found to increase monotonically with the gas fraction (volume of contained gas/volume of foam), the surface tension, and decreasing bubble size (Khan et al. 1988; Gardiner et al. 1998a). Typically, a Herschel–Bulkley model is fitted to the experimental data (Gardiner et al. 1999; Herzhaft et al. 2005).

In the present work, we concentrate our attention on the effects of compressibility assuming that the foam behaves as a homogeneous compressible Newtonian fluid with a viscosity independent of the pressure. The latter assumption is also a strong one; a correct simulation of foam flow has to include pressure-dependent viscosity (Huilgol and You 2006). Beverly and Tanner (1993) were the first to solve numerically the compressible, axisymmetric Newtonian extrudate swell problem. Their simulations showed that weak compressibility reduces the swelling of Newtonian fluids. The finite-element calculations of Georgiou (1995) confirmed this result and showed that, as compressibility increases, the extrudate swell ratio passes through a minimum and then starts increasing rapidly, in agreement with experiments (Behravesh et al. 1998; Park et al. 1998, 1999). A second objective of the present work is to investigate this phenomenon further, given that liquid foams are highly compressible.

First, the governing equations and boundary conditions for the compressible Newtonian extrudate swell flow are presented and discussed. To study the effects of compressibility, two alternative equations of state, a linear and an exponential one, are used. A linear equation of state has been employed in previous numerical studies of the compressible extrudate swell flow (Beverly and Tanner 1993; Georgiou 1995), by Hatzikiriakos and Dealy (1992) for a HDPE, and in our previous studies concerning the simulation of the stick–slip extrusion instability (Georgiou and Crochet 1994; Georgiou 2003). Exponential equations of state have been employed, for example, by Ranganathan et al. (1999) for a HDPE and, more recently, by Vinay et al. (2006), in simulations of weakly compressible Bingham flows. It should be pointed out that taking into account only the pressure dependence of the density (and even that of viscosity) is not sufficient for modeling foam expansion with chemical or physical blowing agents, as these mechanisms involve chemical reaction or gas diffusion, respectively. Because foams are known to slip along the walls (Khan et al. 1988; Enzendorfer et al. 1995; Gardiner et al. 1998b; Gardiner et al. 1999; Bekkour 1999; Bertola et al. 2003; Herzhaft et al. 2005) in addition to the no-slip boundary condition at the wall, the possibility of slip by means of a linear slip equation is also considered. Then, the numerical method is briefly described, and the numerical results are presented and discussed. Emphasis is given on the effects of compressibility on the expansion of the jet. The numerical results confirm previous reports that the swelling of the extrudate decreases initially as the compressibility of the fluid is increased, and then increases considerably in agreement with experimental observations. The numerical simulations also reveal that high compressibility may lead to a contraction of the extrudate after the initial expansion, similar to that observed experimentally with liquid foams or to decaying oscillations of the extrudate surface, provided that inertia is taken into account. Lastly, the conclusions are summarized and some possibilities for future work are given.

Governing equations

Because the equations and boundary conditions for the plane problem are similar, only the axisymmetric extrudate swell flow is discussed. The flow is assumed to be laminar, compressible, and isothermal, and gravity is neglected. Letting p, v, and $\boldsymbol{\tau}$ denote the pressure, the velocity vector, and the viscous stress tensor,

respectively, the continuity and the momentum equations are written as

$$\frac{\partial \rho}{\partial t} + \nabla \cdot \rho v = 0 , \tag{1}$$

$$\rho \left(\frac{\partial v}{\partial t} + v \cdot \nabla v \right) = -\nabla p + \nabla \cdot \boldsymbol{\tau} , \tag{2}$$

where ρ is the density. For compressible Newtonian flow with the bulk viscosity neglected, the viscous stress tensor is given by

$$\boldsymbol{\tau} = \mu \left[(\nabla v) + (\nabla v)^T \right] - \frac{2}{3} \mu I \nabla \cdot v , \tag{3}$$

where I is the unit tensor, μ is the viscosity, and the superscript T denotes the transpose. The viscosity is assumed to be constant and independent of the pressure.

The above equations are completed by a thermodynamic equation of state relating the density to the pressure. At constant temperature and low pressures, the density can be represented by the linear approximation

$$\rho = \rho_0 \left[1 + \beta (p - p_0) \right] , \tag{4}$$

where

$$\beta \equiv -\frac{1}{V_0} \left(\frac{\partial V}{\partial p} \right)_{p_0, T} \tag{5}$$

is the isothermal compressibility assumed to be constant, V is the specific volume, ρ_0 and V_0 are, respectively, the density and the specific volume at a reference pressure p_0, and T is the temperature. For comparison purposes, the following exponential equation is also used:

$$\rho = \rho_0 \, e^{\beta (p - p_0)} . \tag{6}$$

This is equivalent to the linear equation of state for low pressures depending on the value of β. A disadvantage of this equation is the fast growth of the density (for high values of β). On the other hand, the linear model may lead to negative values of the density. Obviously more sophisticated equations of state should be used for highly compressible flows.

To non-dimensionalize the governing equations, we scale the lengths by the radius R, the velocity by the mean velocity U at the inlet of the capillary, the pressure and the stress components by $\mu U/R$, and the density by ρ_0. With these scalings, the continuity and momentum equations become

$$\frac{\partial \rho}{\partial t} + \nabla \cdot \rho v = 0 , \tag{7}$$

and

$$Re \left(\frac{\partial v}{\partial t} + v \cdot \nabla v \right) = -\nabla p + \nabla \cdot \boldsymbol{\tau} , \tag{8}$$

where all variables are now dimensionless, and Re is the Reynolds number defined as

$$Re \equiv \frac{\rho_0 \, U \, R}{\mu} . \tag{9}$$

The linear and the exponential equations of state respectively become

$$\rho = 1 + Bp \tag{10}$$

and

$$\rho = e^{Bp} , \tag{11}$$

where B is the compressibility number,

$$B \equiv \frac{\beta \, \mu \, U}{R} , \tag{12}$$

and the reference pressure has been set to zero. The behavior of the two dimensionless equations of state is illustrated in Fig. 1. The two models are equivalent only if the pressure, p, and the compressibility number, B, are sufficiently low.

The dimensionless boundary conditions of the flow are shown in Fig. 2. To include slip effects, a linear slip equation is employed, the dimensionless form of which is

$$\tau_w = \frac{1}{A} v_w , \tag{13}$$

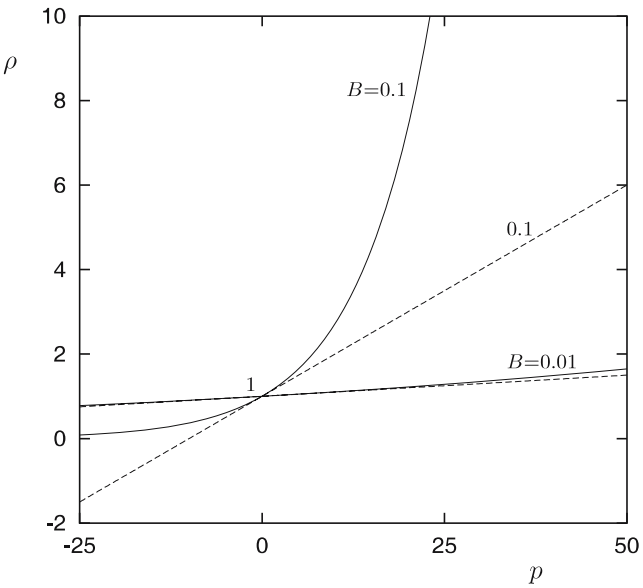

Fig. 1 Behavior of the linear (*dashed*) and exponential (*solid*) equations of state for $B = 0.01$ and 0.1

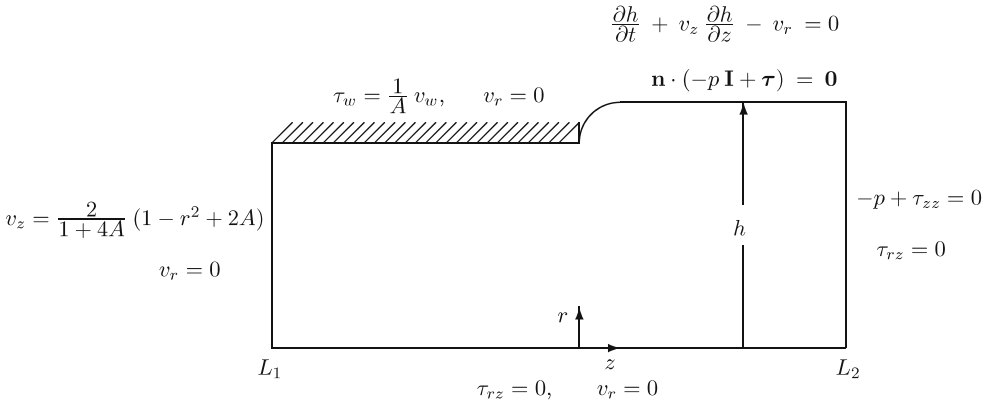

Fig. 2 Geometry and dimensionless boundary conditions for the axisymmetric extrudate swell flow of a Newtonian fluid with slip at the wall

where v_w is the dimensionless slip velocity, τ_w is the dimensionless shear stress at the wall, and A is a dimensionless slip number defined by

$$A \equiv \frac{\alpha\,\mu}{R}\,, \tag{14}$$

α being a slip parameter depending on the material properties for a given wall. Hence, along the capillary wall, the axial velocity, v_z, satisfies the slip equation (13), whereas the radial velocity, v_r, is zero.

At the inlet plane, assumed to be taken far upstream of the exit so that the flow can be taken as fully developed, v_r is zero and v_z is given by

$$v_z = \frac{2}{1 + 4A}\,(1 - r^2 + 2A)\,. \tag{15}$$

The above velocity profile satisfies the slip equation (13). The dimensionless slip velocity at the inlet plane is $v_w = 4A/(1 + 4A)$. Setting $A = 0$ leads to the well-known dimensionless Newtonian velocity profile corresponding to no slip.

The outflow plane is assumed to be far downstream from the die exit so that total normal stress and the shear stress vanish, $-p + \tau_{zz} = 0$ and $\tau_{rz} = 0$. Along the axis of symmetry, the usual symmetry boundary conditions are used. Finally, on the free surface, it is assumed that surface tension is zero and vanishing normal and tangential stresses are imposed. Additionally, the unknown position $h(z, t)$ of the free surface satisfies the kinematic condition:

$$\frac{\partial h}{\partial t} + v_z \frac{\partial h}{\partial z} - v_r = 0\,. \tag{16}$$

In the case of the time-dependent calculations, the solution corresponding to a volumetric flow rate Q_0 at the inlet is used as the initial condition, and at $t = 0$, the volumetric flow rate is perturbed to $Q = 1$.

Numerical simulations

The finite element formulation is used for solving the free-surface flow problem under study. The unknown position of the free surface is calculated simultaneously with the velocity and pressure fields (full-Newton method). The mesh is updated accordingly, using a spine scheme. The standard biquadratic velocity ($P^2 - C^0$) and bilinear-pressure ($P^1 - C^0$) elements with a quadratic representation for the position h of the free surface are employed. For the spatial discretization, the standard Galerkin forms of the continuity, momentum, and kinematic equations are used, while for the time discretization, the standard fully implicit (Euler backward difference) scheme has been chosen.

To check the convergence of the numerical results, we have constructed four meshes of different refinement near the singularity at the die exit. We have also considered three capillary lengths: $L_1 = 5$, 10, and 20. Unless otherwise indicated, the length of the extrudate region has been taken to be $L_2 = 20$. Table 1 shows the sizes of the elements adjacent to the singular point and the characteristics of all meshes used in the present

Table 1 Mesh characteristics

Mesh	L_1	L_2	Size of smaller element	Number of elements	Number of unknowns
Mesh 1	5	20	0.04	3971	37208
Mesh 2	5	20	0.02	4641	43320
Mesh 3	5	20	0.01	5359	49864
Mesh 4	5	20	0.0045	6526	60490
Mesh 3	5	20	0.01	5359	49864
	10	20	0.01	6026	56012
	20	20	0.01	7268	67460
Mesh 3	5	10	0.01	3887	36168
	5	20	0.01	5359	49864
	5	40	0.01	6509	60564

work. In the beginning of this section, we will consider the steady-state creeping flow case. The dramatic effect of inertia will be discussed afterwards.

Creeping flow

We first carried out simulations of the creeping, steady-state axisymmetric extrusion flow with no slip along the capillary wall using the linear equation of state. The effects of mesh refinement on the centerline pressure and the position of the free surface are illustrated in Figs. 3 and 4, respectively, where the results obtained with meshes 1 and 3 for different compressibility numbers are compared. While the calculated centerline pressures practically coincide, the elevation of the free surface is overestimated with the coarser meshes for $B < 0.1$. This is more clearly shown in Fig. 5, where the extrudate swell ratios, h_f, calculated with meshes 1, 2, and 3 are compared. For $B > 0.1$, h_f is underestimated with the coarse meshes. Going back to Fig. 3, we note that the pressure increases with compressibility, which is expected, as the mass flow rate is increased. Test runs for the Poiseuille flow (i.e., with the extrudate region excluded) have shown that the method diverges at high values of B ($B \simeq 0.5$). This observation is useful, as it shows that the divergence of the method in the case of strongly compressible extrusion flow is not due to the sudden elevation of the free surface.

It is clear in Fig. 5 that weak compressibility leads to a small reduction of the extrudate swell ratio, in agreement with earlier numerical studies (Beverly and Tanner 1993; Georgiou 1995). This reduction has been attributed to the compression of the extrudate downstream, given that the fluid is decompressed near the singularity at the die exit where the pressure is negative (Georgiou 1995). However, as compressibility increases, h_f passes through a minimum between $B = 0.02$ and 0.03 and then increases steadily due to the increase of the mass flow rate. At high values of B,

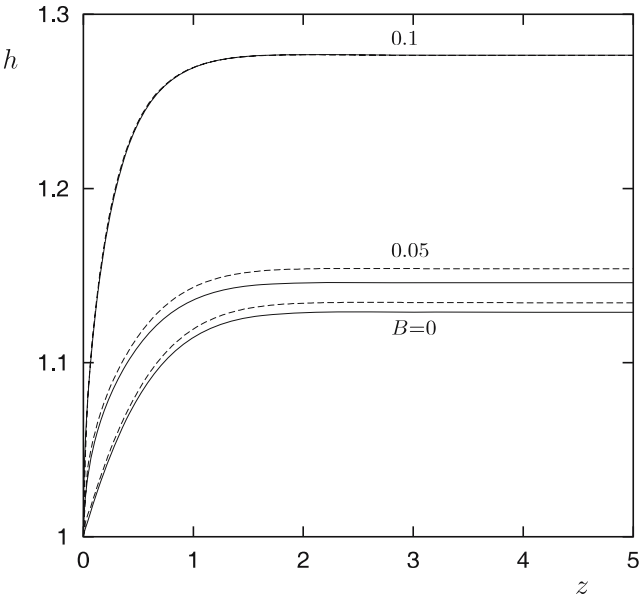

Fig. 4 Effect of mesh refinement on the position of the free surface in creeping axisymmetric flow with no slip at the wall; results obtained with meshes 1 (*dashed*) and 3 (*solid*) and $L_1 = 5$

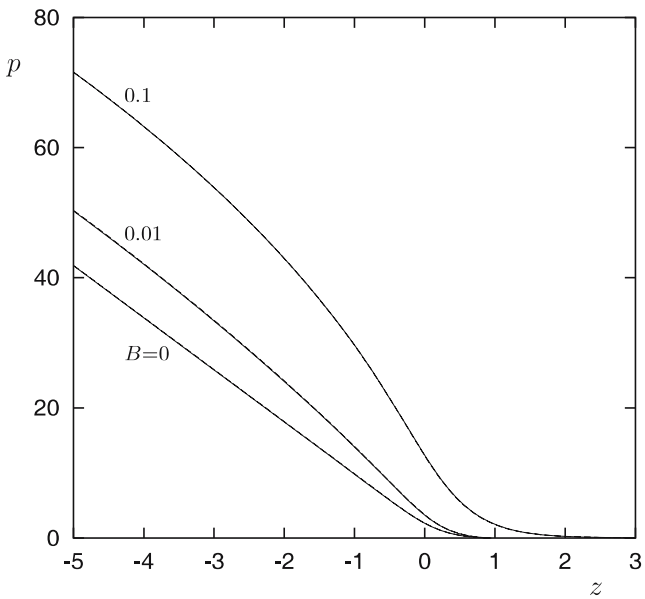

Fig. 3 Effect of mesh refinement on the centerline pressure in creeping axisymmetric flow with no slip at the wall; results obtained with meshes 1 (*dashed*) and 3 (*solid*) and $L_1 = 5$

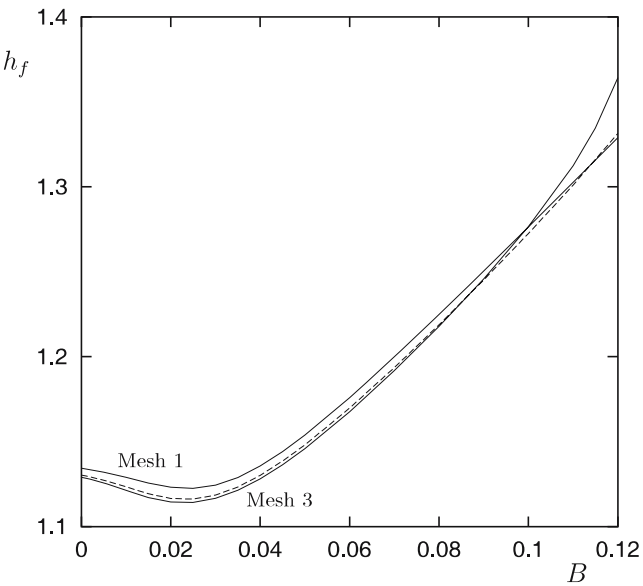

Fig. 5 Effect of mesh refinement on the extrudate swell ratio in creeping axisymmetric flow with no slip at the wall; results obtained with meshes 1, 2 (*dashed*) and 3 and $L_1 = 5$

the angle of expansion increases, and the elevation of the free surface is rapid (see Fig. 4). As already mentioned, the numerical method cannot converge for $B \simeq 0.12$. From Fig. 5, we conclude that the results for $B > 0.08$ should be ignored. In any case, the numerical results show that swelling increases considerably with compressibility, in agreement with foam extrusion experiments (Behravesh et al. 1998; Park et al. 1998, 1999).

The expansion of the jet is further enhanced by increasing the capillary length, while it is reduced when slip occurs along the capillary wall. As illustrated in Fig. 6, the minimum of the extrudate swell ratio is shifted to the left, and higher extrudate swell ratios are obtained when the length of the capillary, L_1, is increased, as more material is compressed. It should be noted that increasing the capillary length leads to a higher mass flow rate (as the velocity scale is the same), and therefore, the mean velocity at the exit is higher. Figure 7 shows the effect of slip on the free surface profile for $B = 0.06$. Swelling is reduced as slip is increased, which is consistent with experiments and theoretical studies.

Let us now look more closely at the numerical solution of strongly compressible flow. In Fig. 8, we see the finite element mesh, the velocity and pressure contours, and the streamlines obtained with mesh 3 ($L_1 = 10$) for $B = 0.08$. Two interesting observations are that (a) the free surface is almost vertical near the exit, and (b) there is a big region in the extrudate region where the pressure is negative, i.e., the density is less than the reference density. The negative pressures are swept out because of the convective nature of the flow.

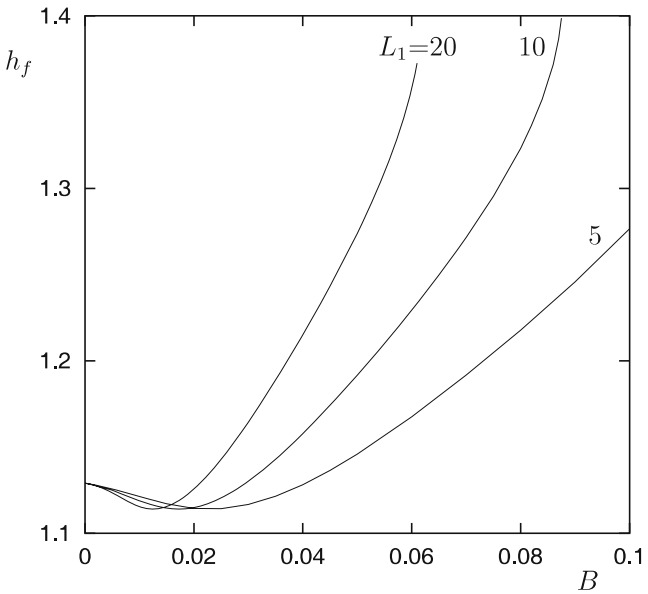

Fig. 6 Effect of the capillary length on the extrudate swell ratio in creeping axisymmetric flow with no slip at the wall

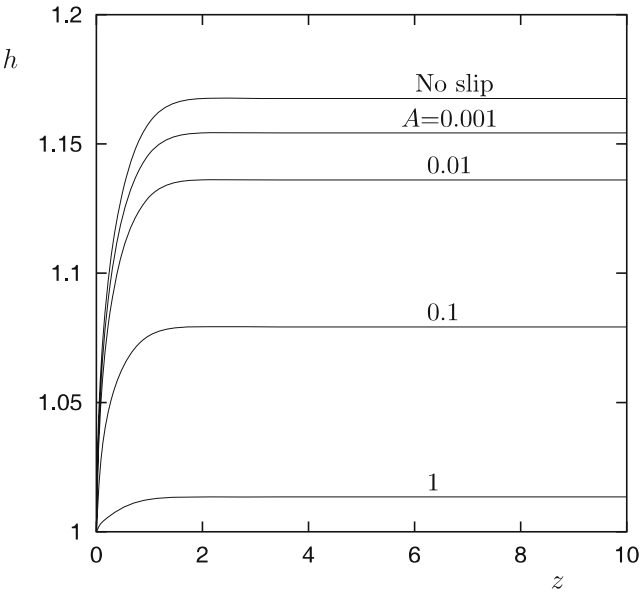

Fig. 7 Free surface profiles for $B = 0.06$ and different slip numbers in creeping axisymmetric flow; mesh 3 with $L_1 = 5$ and $L_2 = 20$

The results with the exponential equation of state showed the importance of using a proper equation of state in the simulations. In Fig. 9, the centerline pressures from $B = 0$ (incompressible flow) up to $B = 0.025$, calculated with $L_1 = 5$, are plotted. The results for $B < 0.01$ are essentially the same as those obtained with the linear equation of state and shown in Fig. 3. For higher values of B, however, the pressure increases rapidly and the numerical method fails to converge for $B > 0.025$. In Fig. 10, the extrudate-swell ratios calculated with the two equations of state are compared. Again, for $B < 0.01$, both equations yield essentially the same results. With the exponential equation of state, the minimum is again observed, but at a lower compressibility number. Just after the minimum, the extrudate-swell ratio increases considerably due to the dramatic increase of the pressure and, hence, the mass flow rate.

The numerical results for the planar compressible extrudate-swell flow are similar. In Fig. 11, we compare to their axisymmetric counterparts the extrudate swell ratios obtained with Mesh 3 and $L_1 = 5$. With the same mesh, simulations of the planar flow can be carried out for higher values of the compressibility number. Again, the extrudate swell ratio passes through a minimum, but at a higher compressibility number around $B = 0.05$. It should be noted that for $B > 0.06$ the planar jet swells less than the axisymmetric one.

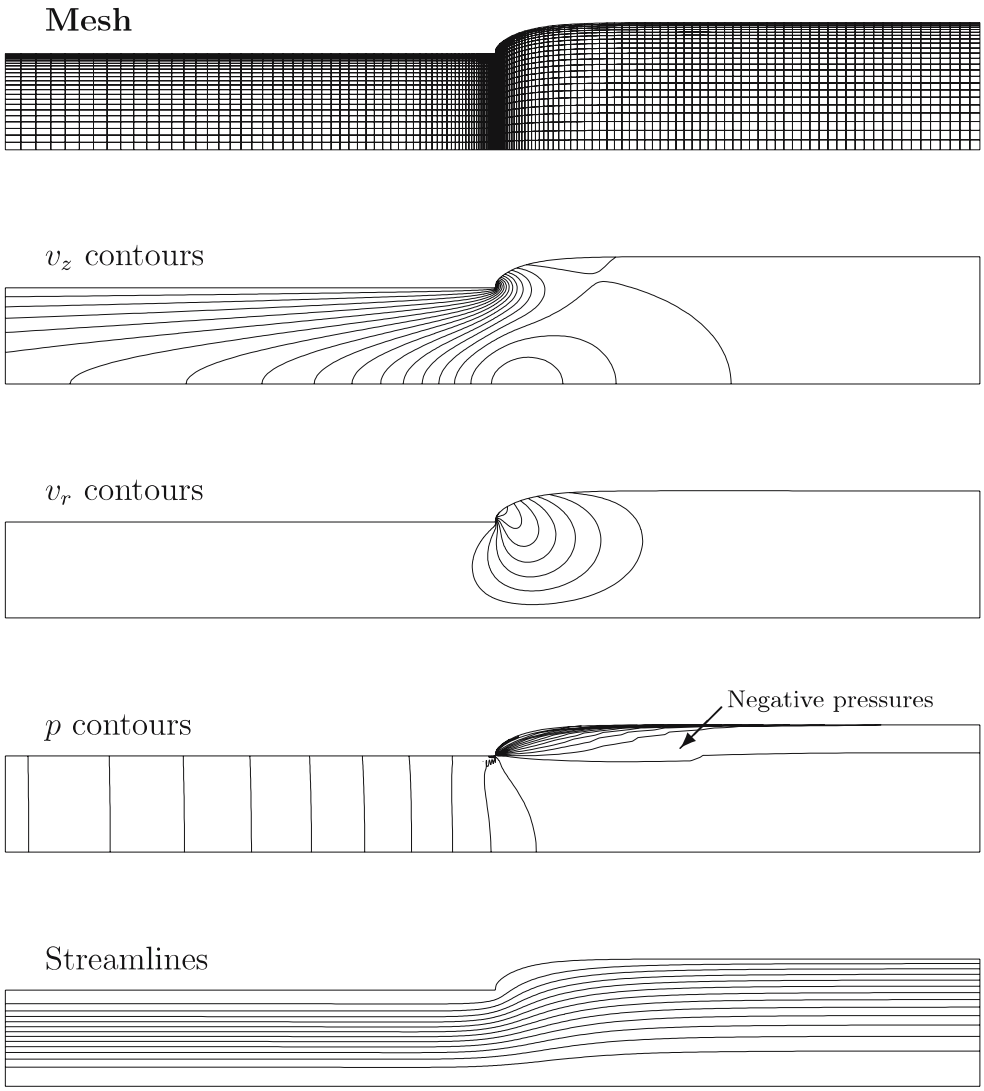

Fig. 8 Mesh and contours in creeping compressible axisymmetric extrudate swell flow with no slip at the wall; $B = 0.08$, $L_1 = 10$ (only part of the domain is shown)

We have also studied the effect of compressibility on the pressure exit correction factor which gives the relative excess pressure loss above the Poiseuille fully-developed pressure loss. This is defined as follows (Tanner 2000):

$$n_{ex} = \frac{\Delta P - \Delta P_0}{2\,\sigma_w} \tag{17}$$

where ΔP is the pressure drop between the inlet plane and the exit in the case of the extrudate swell flow, ΔP_0 is the pressure drop between the inlet plane and the exit of the capillary in the case of fully-developed Poiseuille flow, and σ_w is the wall shear stress corresponding to incompressible Poiseuille flow. In the present work, the pressure differences are taken along the centerline. The exit correction factors for both the planar and the axisymmetric flows are found to increase with compressibility, as shown in Fig. 12. The increase is more dramatic in the case of the axisymmetric flow. The convergence of these results has been checked by using meshes 1 to 4. In Table 2, the calculated exit correction factors for both the axisymmetric and planar incompressible flows are tabulated together with the corresponding extrudate swell ratios. The convergence of n_{ex} with mesh refinement is illustrated in Fig. 13. It appears that the converged values of n_{ex} are about 0.227 for the axisymmetric jet and 0.147 for the planar one. These values, which are insensitive to the capillary length L_1 (for $L_1 > 3$), are much lower than those reported in the literature (Mitsoulis 1986; Tanner 2000). However, as pointed out by Mitsoulis (1986), who reported the value $n_{ex} = 0.235$ for the axisymmetric jet, coarse meshes tend to overestimate n_{ex}, which is consistent with the present calculations. We believe that the meshes used in previous studies were rather coarse. Finally, as the mesh size is decreased the computed values of the

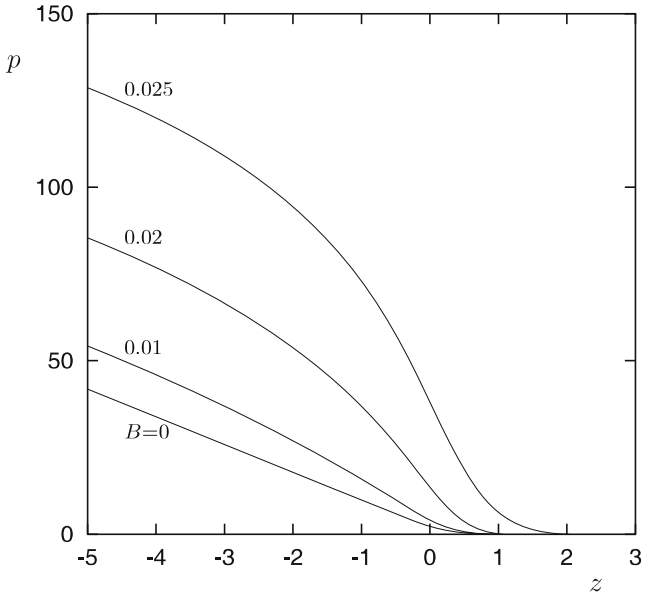

Fig. 9 Centerline pressures calculated with the exponential equation of state for different compressibility numbers; creeping axisymmetric flow with no slip at the wall, mesh 3 with $L_1 = 5$

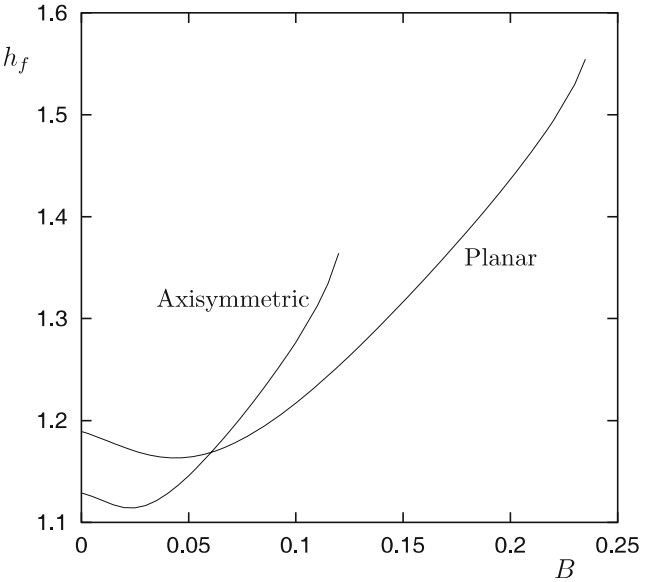

Fig. 11 Calculated extrudate swell ratios for both the axisymmetric and planar extrudate swell flows; creeping flow with no slip at the wall, Mesh 3 with $L_1 = 5$

extrudate swell ratio (tabulated in Table 2) appear to approach nicely the converged values 1.1265 and 1.1863 reported by Georgiou and Boudouvis (1999) for the axisymmetric and planar flows, respectively.

Effect of inertia

It is well known that, in the incompressible case ($B=0$), swelling is reduced as the Reynolds number is increased (Georgiou et al. 1988). Our simulations showed that this is also the case with weakly compressible flows. At high compressibility numbers, however, the final extrudate swell ratio increases sharply with the Reynolds number, as illustrated in Fig. 14, which shows results obtained with the no-slip boundary condition. In some intermediate range of compressibility numbers, the final extrudate swell ratio appears to pass through a minimum.

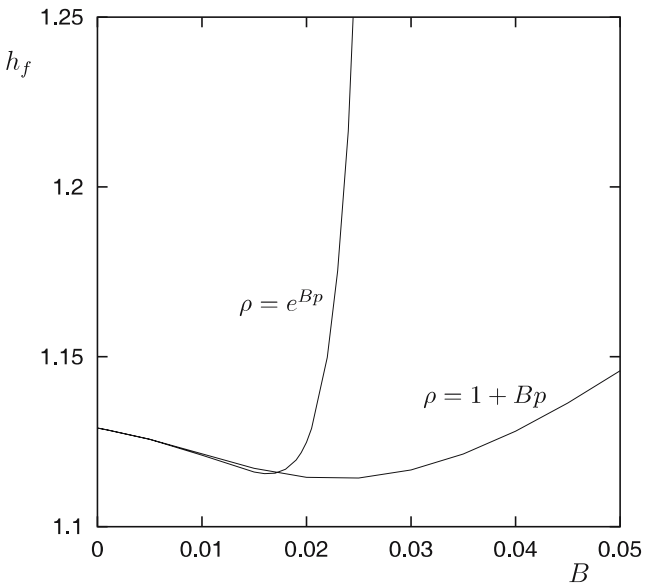

Fig. 10 Calculated extrudate swell ratios with the two equations of state; creeping axisymmetric flow with no slip at the wall, mesh 3 with $L_1 = 5$

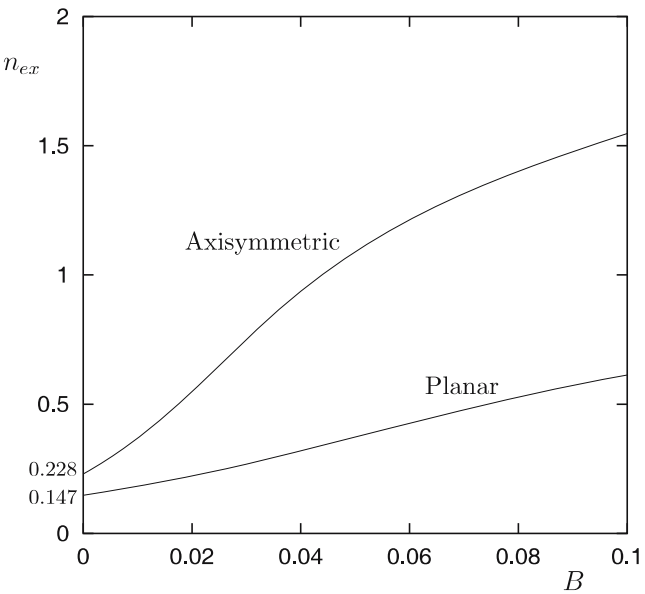

Fig. 12 Exit correction factors for both the axisymmetric and extrudate-swell flows versus the compressibility number; creeping flow with no slip at the wall, Mesh 3 with $L_1 = 5$

Table 2 Convergence of the exit correction factor and the extrudate swell ratio with mesh refinement

Mesh	Size of	Axisymmetric		Planar	
	smaller element	n_{ex}	h_f	n_{ex}	h_f
Mesh 1	0.04	0.23603	1.1344	0.15139	1.1953
Mesh 2	0.02	0.23191	1.1303	0.14909	1.1908
Mesh 3	0.01	0.23021	1.1290	0.14816	1.1893
Mesh 4	0.0045	0.22855	1.1278	0.14725	1.1878

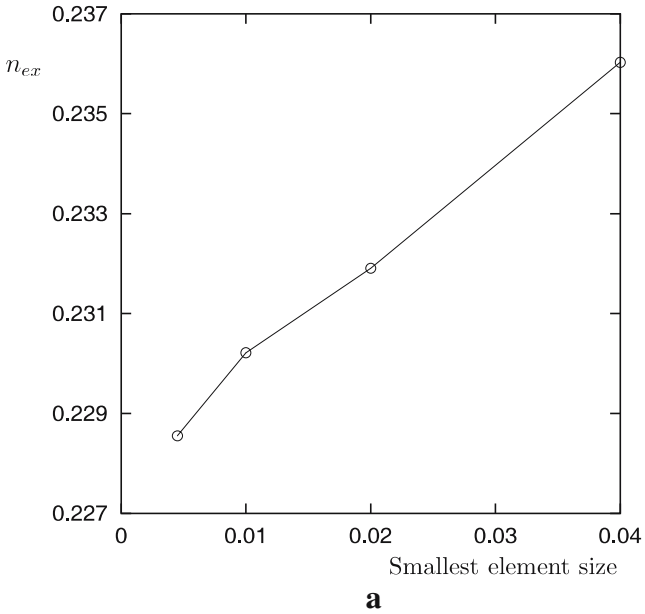

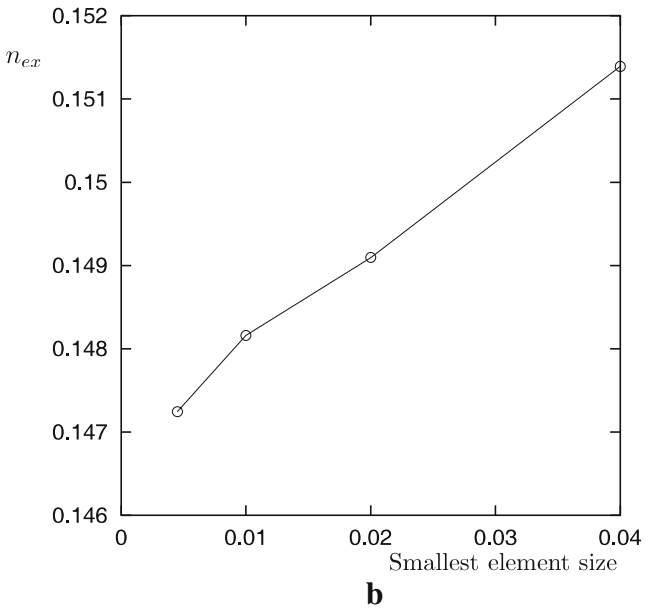

Fig. 13 Convergence of the exit pressure correction factor with mesh refinement: **a** Axisymmetric jet, **b** planar jet; creeping flow with no slip at the wall, mesh 3 with $L_1 = 5$

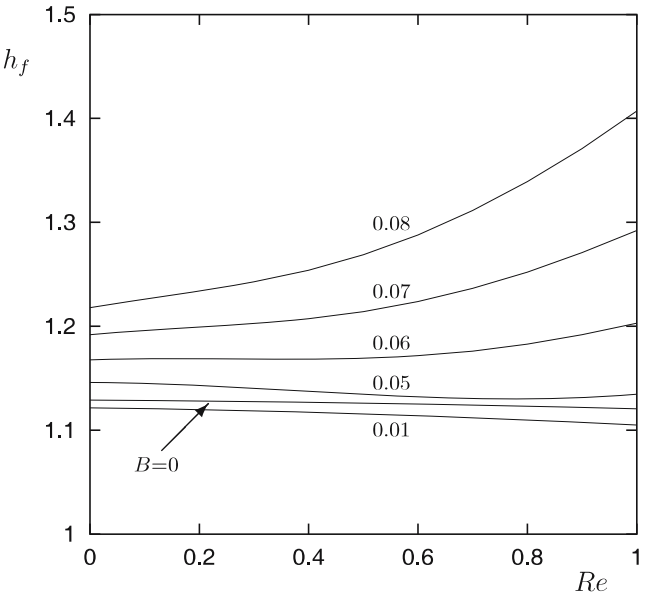

Fig. 14 Final extrudate swell ratio vs Re for different compressibility numbers; axisymmetric flow with no slip at the wall, mesh 3 with $L_1 = 5$ and $L_2 = 20$

The free-surface profiles for nonzero Reynolds number look more exciting than the values of the final extrudate swell ratio. In Figs. 15 and 16, the free-surface profiles for $B = 0.06$ and $B = 0.08$, respectively, and various Reynolds numbers are shown. We observe that the angle of expansion and the swelling increase with the Reynolds number and that the expansion is followed by a weaker contraction. This behavior of the free surface agrees with the experimental obser-

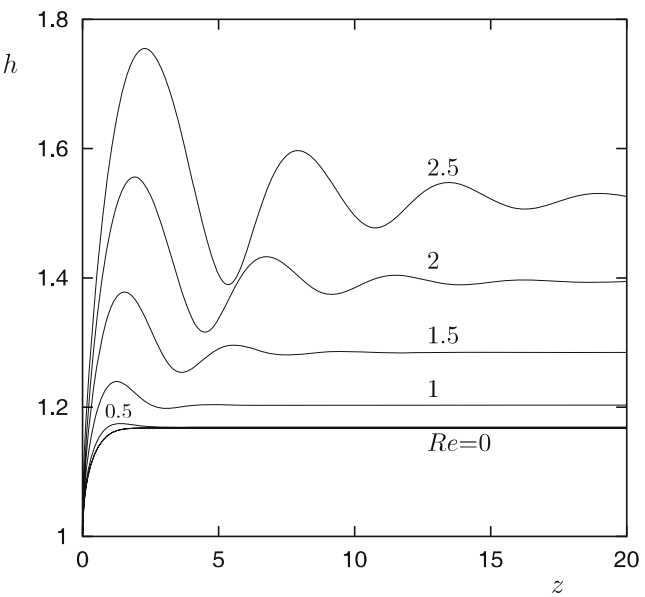

Fig. 15 Free surface profiles for $B = 0.06$ and different Reynolds numbers; axisymmetric flow with no-slip at the wall, mesh 3 with $L_1 = 5$ and $L_2 = 20$

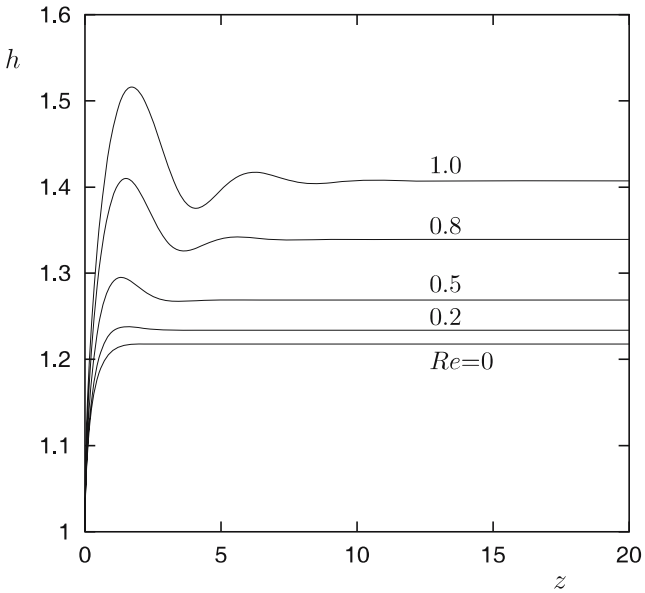

Fig. 16 Free-surface profiles for $B = 0.08$ and different Reynolds numbers; axisymmetric flow with no slip at the wall, mesh 3 with $L_1 = 5$ and $L_2 = 20$

vations on extruded polymer (Behravesh et al. 1998; Park et al. 1998; Naguib et al. 2004; Naguib et al. 2006), starch-based (Fan et al. 1994; Willett and Shogren 2002; Wang et al. 2005; Xu and Hanna 2005) and cereal (Moraru and Kokini 2003) foams. Therefore, the phenomenon of foam extrudate contraction can, at least partially, be attributed to the combined effect of the compressibility of the foam and inertia.

As the Reynolds number is further increased, more decaying oscillations of the free surface are observed downstream. The same phenomenon is observed when the fluid is allowed to slip along the capillary wall. In Fig. 17, we plot the free-surface profiles obtained for $B = 0.06$, $A = 0.1$, and various Reynolds numbers. A comparison with Fig. 15 shows again that slip reduces swelling and the amplitude of the free-surface oscillations.

The effect of compressibility for a nonzero Reynolds number ($Re = 1$) is illustrated in Fig. 18, where steady free-surface profiles obtained with different values of B are shown. The free surface is monotonic in the incompressible case. As in the creeping flow, the angle of expansion and swelling increase with B. A kink appears that grows with B. At higher compressibilities, there appear smaller decaying oscillations after the initial kink. Figure 19 shows the mesh and the axial velocity contours when $B = 0.06$ and $Re = 2.5$ (i.e., a rather extreme case). The sharp angle of expansion, as well as the dense refinement of the mesh in the axial direction, are clear.

Some checks have been considered to confirm that the calculated oscillating steady free-surface profiles are not numerical artifacts. First, we verified that the solution does not depend on the length L_2 of the extrudate. Figure 20 shows comparisons of the free-surface profiles obtained for $B = 0.06$, various Reynolds numbers, and $L_2 = 10$, 20, and 40. It is clear that the results coincide in all cases. In other words, the oscillatory

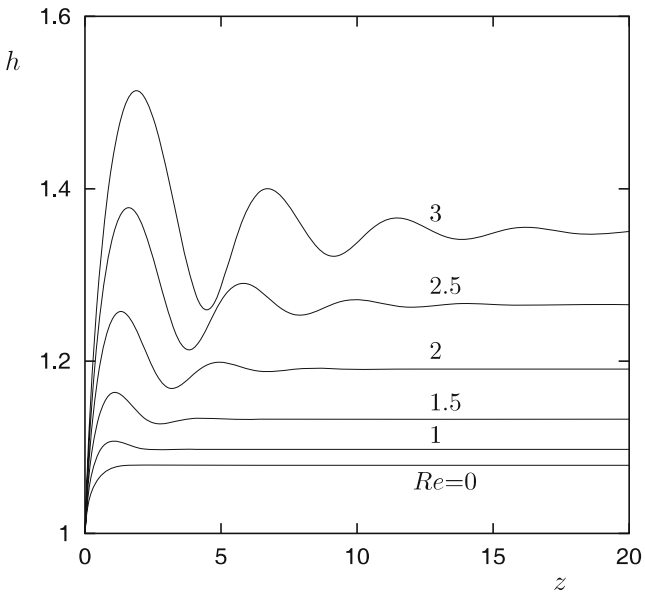

Fig. 17 Free surface profiles for $B = 0.06$, $A = 0.1$, and various Reynolds numbers; axisymmetric flow, mesh 3 with $L_1 = 5$ and $L_2 = 20$

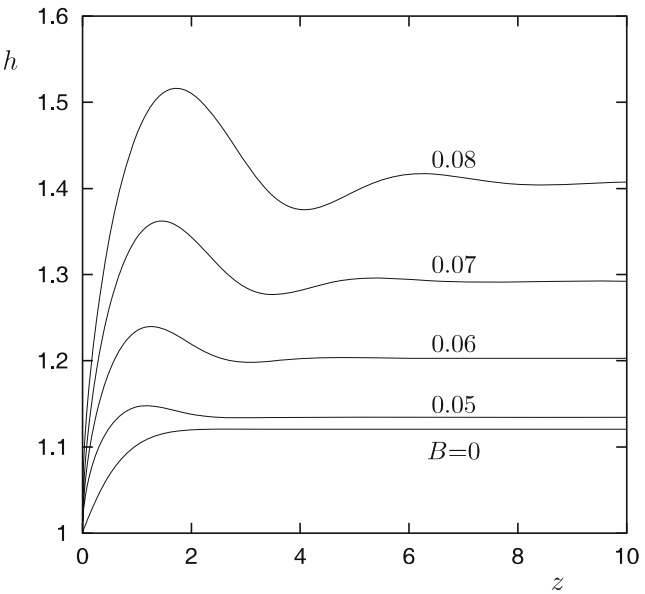

Fig. 18 Free-surface profiles for $Re = 1$ and different compressibility numbers; axisymmetric flow with no slip at the wall, mesh 3 with $L_1 = 5$ and $L_2 = 20$

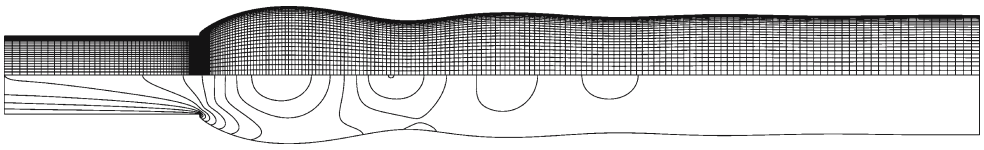

Fig. 19 Mesh and axial velocity contours for $B = 0.06$ and $Re = 2.5$; axisymmetric flow with no slip at the wall, mesh 3 with $L_1 = 5$ and $L_2 = 20$

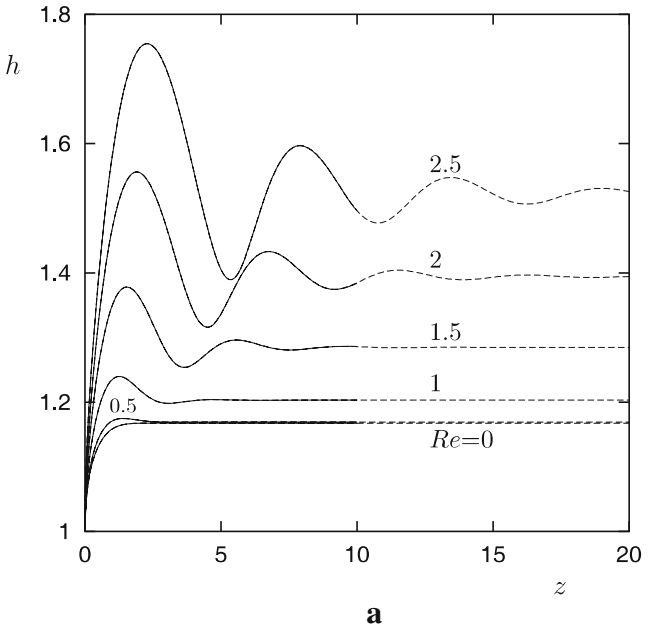

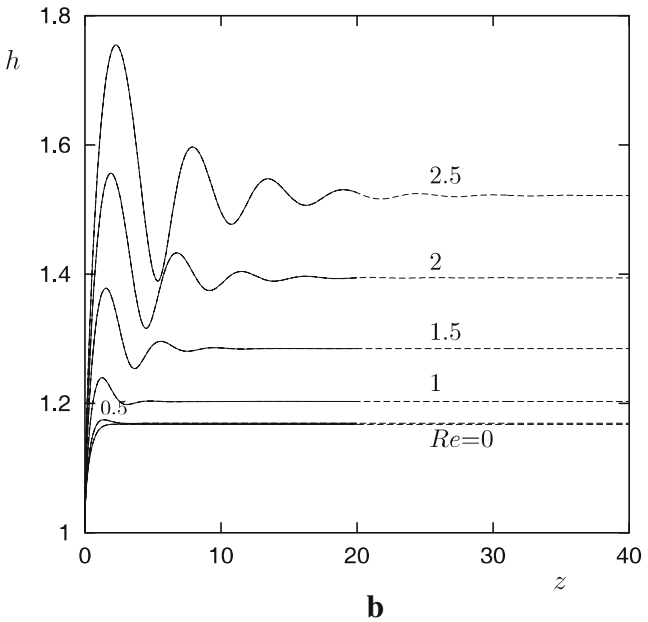

Fig. 20 Effect of the extrudate length on the steady free-surface profiles for $B = 0.06$ and various Reynolds numbers: **a** results for $L_2 = 10$ (*solid*) and 20 (*dashed*); **b** results for $L_2 = 20$ (*solid*) and 40 (*dashed*); axisymmetric flow with no slip at the wall, mesh 3 with $L_1 = 5$

nature of the steady-state solutions is not affected by the length of the extrudate.

We have also checked the stability of the oscillatory steady-state solutions by means of time-dependent calculations. The steady-state solution at the volumetric flow rate $Q_0 = 0.5$ has been taken as the initial condition, and at $t = 0$ the volumetric flow rate was set to $Q = 1$. In all cases examined, the oscillatory steady states have been found to be stable. A rather extreme example for $B = 0.06$ and $Re = 2.5$ is presented in this paper. The free surface profiles for $Q_0 = 0.5$ and $Q = 1$ are shown in Fig. 21. In Fig. 22, the evolution of the free surface to the new oscillatory steady state is shown. The large free-surface profile overshoot, which is due to the sudden increase of the volumetric flow rate, propagates downstream, and the new stable steady state is finally reached.

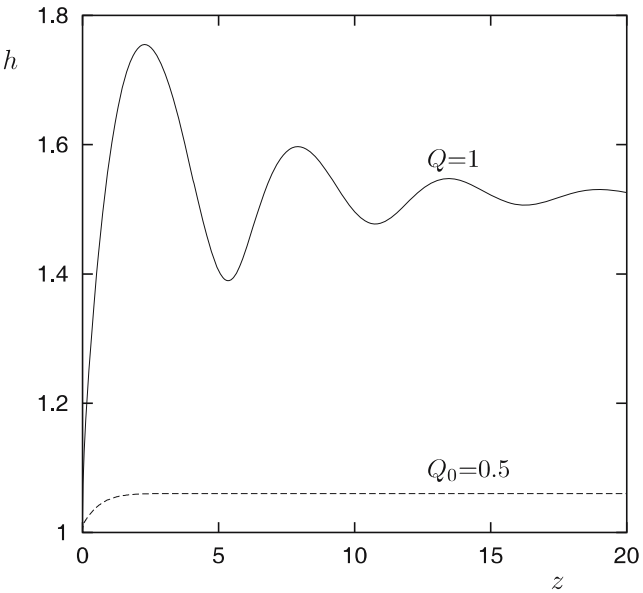

Fig. 21 Steady free-surface profiles for $B = 0.06$, $Re = 1$, $Q_0 = 0.5$ (initial condition), and $Q = 1$ (new steady-state); axisymmetric flow with no slip at the wall, mesh 3 with $L_1 = 5$ and $L_2 = 20$

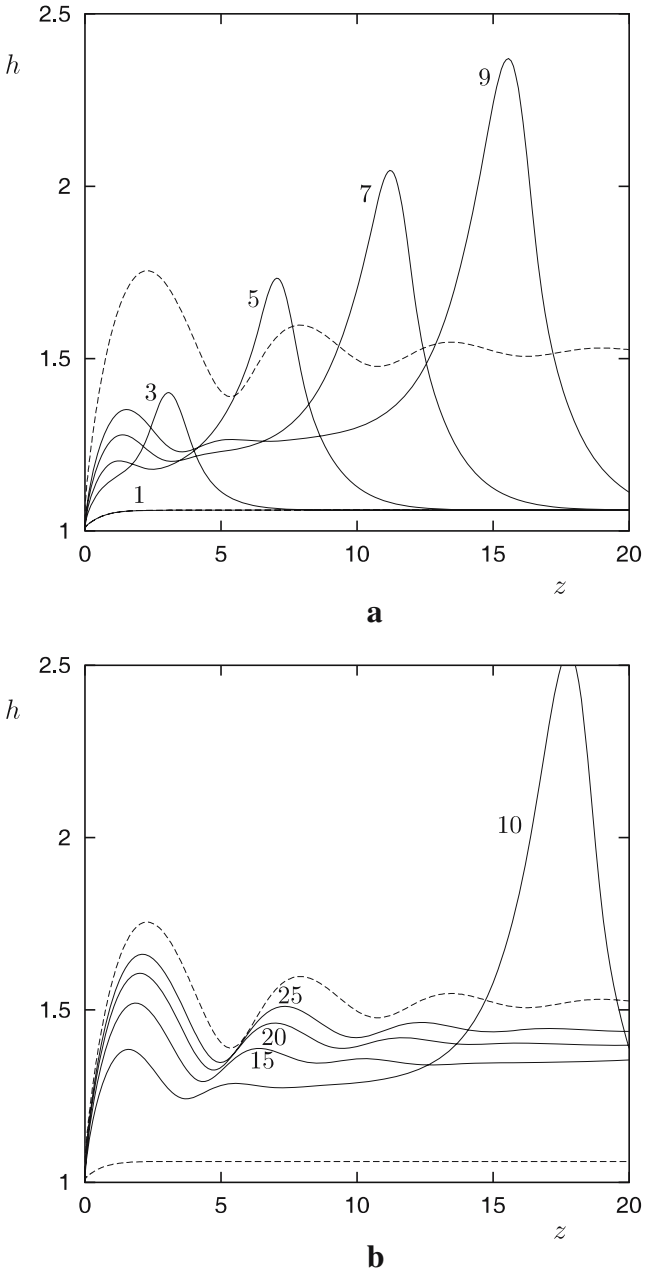

Fig. 22 Evolution of the free surface when perturbing the steady-state solution for B=0.06 and $Re = 2.5$ from $Q_0 = 0.5$ to $Q = 1$: **a** $t = 1, 3, 5, 7$, and 9; **b** $t = 10, 15, 20, 25$; the *dashed lines* show the initial and the final steady state; axisymmetric flow with no slip at the wall, mesh 3 with $L_1 = 5$ and $L_2 = 20$

Conclusions

We have solved numerically the axisymmetric and plane extrudate swell flows of a strongly compressible Newtonian fluid and studied the effects of the compressibility and the equation of state, slip, geometry, and inertia on the expansion of the jet. In agreement with experimental observations (Behravesh et al. 1998; Park et al. 1998, 1999), strong compressibility was found to enhance the expansion and the angle of separation of the jet. However, swelling initially decreases as compressibility is increased, which agrees with previous numerical studies (Beverly and Tanner 1993; Georgiou 1995). The expansion of the jet is further enhanced when the length of the capillary is increased, i.e., when more material is compressed. On the other hand, slip at the wall reduces swelling. The planar jet has been found to swell more than its axisymmetric counterpart only below a certain value of the compressibility number. The simulations with a linear and an exponential equation of state showed that swelling is accelerated in the latter case, which indicates the importance of using a more physically based equation of state. We are currently investigating this issue in conjunction with the use of a more realistic constitutive equation for liquid foams, such as the Herschel–Bulkley model with density-dependent parameters. Another consideration is the construction of the finite element mesh that needs to be improved to capture the high expansion ratios observed in foam extrusion experiments.

The numerical simulations for non-zero Reynolds number revealed that compressibility leads to a contraction of the jet after the initial expansion, a phenomenon that has been observed in extrusion experiments with polymer (Behravesh et al. 1998; Park et al. 1998; Naguib et al. 2004; Naguib et al. 2006), starch-based (Fan et al. 1994; Willett and Shogren 2002; Wang et al. 2005; Xu and Hanna 2005), and cereal (Moraru and Kokini 2003) foams. At higher Reynolds numbers, the steady-state free-surface profiles become oscillatory, with the oscillations decaying downstream. These steady-state oscillatory solutions are not affected by the length of the extrudate region nor by the boundary condition along the capillary wall (slip or no-slip). Their stability has been confirmed by means of time-dependent calculations.

Acknowledgment This work was made possible under the "Socrates" inter-university exchange program between Greece and Cyprus. Its financial assistance is gratefully acknowledged.

References

Behravesh AH, Park CB, Venter RD (1998) Challenge to the production of low-density, fine-cell HDPE foams using CO_2. Cell Polym 17:309

Bekkour K (1999) Evaluation of slip effects in the capillary flow of foams. Appl Rheol 9:10
Belkessam O, Fritsching U (2003) Modelling and simulation of continuous metal foaming process. Model Simul Mat Sci Eng 11:823
Bertola V, Bertrand F, Tabuteau H, Bonn D, Coussot P (2003) Wall slip and yielding in pasty materials. J Rheol 47:1211
Beverly CR, Tanner RI (1993) Compressible extrudate swell. Rheol Acta 35:526
Enzendorfer C, Harris RA, Valkó P, Economides MJ, Fokker PA, Davies DD (1995) Pipe viscometry of foams. J Rheol 39:345
Fan J, Mitchell JR, Blanshard JMV (1994) A computer simulation of the dynamics of bubble growth and shrinkage during extrudate expansion. J Food Eng 23:337
Gardiner BS, Dlugogorski BZ, Jameson GJ (1998a) Yield stress measurements of aqueous foams in the dry limit. J Rheol 42:1437
Gardiner BS, Dlugogorski BZ, Jameson GJ (1998b) Rheology of fire-fighting foams. Fire Saf J 31:61
Gardiner BS, Dlugogorski BZ, Jameson GJ (1999) Prediction of pressure losses in pipe flow of aqueous foams. Ind Eng Chem Res 38:1099
Georgiou GC, Papanastasiou TC, Wilkes JO (1988) Laminar jets at high Reynolds and high surface tension. AIChE J 34:1559
Georgiou GC, Crochet MJ (1994) Compressible viscous flow in slits with slip at the wall. J Rheol 38:639
Georgiou GC (1995) The compressible Newtonian extrudate swell problem. Int J Numer Methods Fluids 20:255
Georgiou GC, Boudouvis A (1999) Converged solutions of the Newtonian extrudate swell problem. Int J Numer Methods Fluids 29:363
Georgiou G (2003) The time-dependent compressible Poiseuille and extrudate-swell flows of a Carreau fluid with slip at the wall. J Non-Newton Fluid Mech 109:93
Hatzikiriakos SG, Dealy JM (1992) Role of slip and fracture in the oscillating flow of a HDPE in a capillary. J Rheol 36:845
Herzhaft B, Kakadjian S, Moan M (2005) Measurement and modeling of the flow behavior of aqueous foams using a recirculating pipe rheometer. Colloids Surf A Physicochem Eng Asp 263:153
Höhler R, Cohen-Addad S (2005) Rheology of liquid foam. J Phys Condens Matter 17:R1041
Huilgol RR, You Z (2006) On the importance of the pressure dependence of viscosity in steady non-isothermal shearing flows of compressible and incompressible fluids and in the isothermal fountain flow. J Non-Newton Fluid Mech 136:106
Khan SA, Schnepper CA, Armstrong RC (1988) Foam rheology: III. Measurement of shear flow properties. J Rheol 32:69
Kraynik AM (1988) Foam flows. Annu Rev Fluid Mech 20:325
Lee PC, Wang J, Park CB (2006) Extrusion of microcellular open-cell LDPE-based sheet foams. J Appl Polym Sci 102:3376
Mitsoulis E (1986) The numerical simulation of Boger fluids: a viscometric approximation approach. Polymer Eng Sci 26:1552
Moraru CI, Kokini JL (2003) Nucleation and expansion during extrusion and microwave heating of cereal foods. Compr Rev Food Sci Food Saf 2:120
Naguib HE, Park CB, Reichelt N (2004) Fundamental foaming mechanisms governing the volume expansion of extruded polypropylene foams. J Appl Pol Sci 91:2661
Naguib HE, Park CB, Lee PC, Xu D (2006) A study on the foaming behaviors of PP resins with talc as nucleating agent. J Polymer Eng 26:565
Park CB, Behravesh AH, Venter RD (1998) Low density microcellular foam processing in extrusion using CO_2. Polymer Eng Sci 38:1812
Park CB, Liu Y, Naguib HE (1999) Challenge to forty-fold expansion of biodegradable polyester foams using carbon dioxide as a blowing agent. Cell Polym 18:367
Ranganathan M, Mackley MR, Spitteler PHJ (1999) The application of the multipass rheometer to time-dependent capillary flow measurements of a polyethylene melt. J Rheol 43:443
Reinelt DA, Kraynik AM (2000) Simple shearing flow of dry soap foams with tetrahedrally close-packed structure. J Rheol 44:453
Sokhey AS, Ali Y, Hanna MA (1997) Effects of die dimensions on extruder performance. J Food Eng 31:251
Tanner RI (2000) Engineering rheology. Oxford University Press, Oxford
Vinay G, Wachs A, Agassant JF (2006) Numerical simulation of weakly compressible flows: the restart of pipeline flows of waxy crude oils. J Non-Newton Fluid Mech 136:93
Wang L, Canjyal GM, Jones DD, Weller CL, Hanna MA (2005) Modeling of bubble growth dynamics and nonisothermal expansion in starch-based foams during extrusion. Adv Polym Technol 24:29
Willett JL, Shogren RL (2002) Processing and properties of extruded starch/polymer foams. Polymer 43:5935
Xu X, Park CB, Xu D, Pop-Iliev R (2003) Effects of die geometry on cell nucleation of PS foams blown with CO_2. Polym Eng Sci 43:1378
Xu Y, Hanna MA (2005) Preparation and properties of biodegradable foams from starch acetate and poly (tetramethylene adipate-co-terephthalate). Carbohydr Polym 59:521
Xu Z, Xue P, Zhu F, He J (2005) Effects of formulations and processing parameters on foam morphologies in the direct extrusion foaming of polypropylene using a single-screw extruder. J Cell Plast 41:169